IEEE Access
Multidisciplinary | Rapid Review | Open Access Journal

Received May 8, 2020, accepted July 2, 2020, date of publication July 6, 2020, date of current version July 22, 2020.

*Digital Object Identifier 10.1109/ACCESS.2020.3007486*

# A Transient Bulging Phenomenon in Fast Doping Processes for p-n Junctions

**JIHONG ZHANG[1] AND TIENMO SHIH[2,3]**

[1]School of Electromechanical and Automotive Engineering, Yantai University, Yantai 264005, China
[2]Department of Physics, Xiamen University, Xiamen 361005, China
[3]Tianming Physics Research Institute, Changtai 363900, China

Corresponding author: Tienmo Shih (tienmoshih@gmail.com)

This work was supported in part by the National Natural Science Foundation of China under Grant 11604285, in part by the Natural Science Foundation of Shandong Province under Grant ZR2016FQ11, in part by the International Science and Technology Cooperation Program of China under Grant 2015DFG62190, in part by the Major Science and Technology Project between University-Industry Cooperation in Fujian Province under Grant 2013H6024, in part by the National Natural Science Foundation of China under Grant 61504112 and Grant 11604285, in part by the Natural Science Foundation of Shandong Province under Grant ZR2016FQ11, in part by the Natural Science Foundation of Fujian Province under Grant 2016R0091, and in part by the Zing Semiconductors in Shanghai.

**ABSTRACT** During transient stages, under fast doping processes, the minor-carrier transport can affect the major-carrier counterpart in a peculiar manner. In this study, we have numerically detected occurrences of carrier-concentration bulges, which confine electrons both locally and instantaneously (for several nanoseconds). The governing mechanism, in which electrical fields, subtly actuated by the early minority-carrier arrival, account for unbalanced forces that then oppose the majority-carrier diffusion, has been further identified. To calibrate our in-house computer code, we have conducted experiments to measure steady-state carrier spatial distributions, which agree satisfactorily with our numerical results. Our finding may shed light on future studies that primarily investigate the nonlinearity coupling between the electron transport and the hole counterpart.

**INDEX TERMS** Fast doping processes, carrier-concentration bulges, major-carrier, majority-carrier.

## I. INTRODUCTION

Drift, diffusion, generation, and recombination of electron-hole paired carriers strongly affect performances of most semiconductor devices in areas of light emission, transistor designs, as well as electricity generation, and have been intensively studied since several decades ago experimentally, theoretically, and numerically [1]–[6]. In particular, in their pioneering study, Queisser *et al.* have presented current-voltage characteristics and potential distributions for GaAs p-n junctions, focusing on comparisons between the carrier lifetime and the dielectric relaxation time [1]. Fundamentally, carrier temporal and spatial concentrations in p/n junctions are governed by partial differential equations that obey carrier conservations as well as the relationship between the voltage and the electrical field [7]. In practical doping processes (e. g. metalorganic chemical vapor deposition), the p/n junction manufacturing is established gradually based on various epitaxial growth model, typified by Frank - Van der Merwe [8], Volmer – Weber[9], and Stranski - Krastanow [10], such that a sufficient period of time has elapsed to allow electrons (minor carrier) to diffuse into the p-type semiconductor and holes (minor carrier) to diffuse into the n-type semiconductor. In previous reports, P-N junctions have been realized by applying separate gates to locally induce hole and electron doping in 2D materials, such as graphene [11]–[13] and black phosphorous [14], [15]. Although carrier dynamics have been investigated theoretically by non-equilibrium Green function [16] and experimentally by ultrafast transient absorption and photocurrent microscopy in 2D materials [17], [18] and bulk semiconductors [19], [20], research on carrier concentrations during the ultrafast doping process has been rarely reported, since it is difficult to dope bulk semiconductors in high doping velocities (defined as the doping penetration depth per unit time) without defects in the current doping technology. The transient carrier concentration caused by ultrafast doping process in bulk

The associate editor coordinating the review of this manuscript and approving it for publication was Jenny Mahoney.

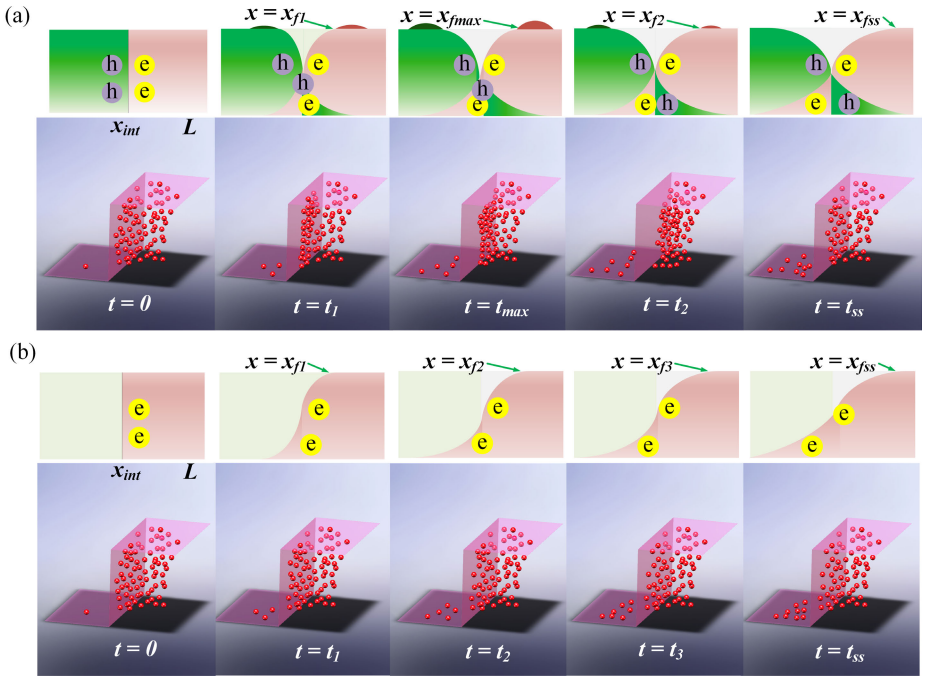


**FIGURE 1.** System schematic and related features. a, Various transient stages of carrier spatial distributions inside the p/n junction. b, only the transport of the n carrier is considered, showing absolutely no bulges.

semiconductors will be intriguing, and can be investigated in theory as well as calibrated by experiments in steady state. As a result, we have theoretically examined cases in which the doping velocities is infinite, therefore, both concentrations of electrons and holes are distributed uniformly at the initial time. In such a doping process, due to the nonlinear coupling in diffusion terms, bulge phenomena in transient stages have unexpectedly occurred and lasted for a few nanoseconds. Here, we report these intriguing phenomena in detail, and also discuss the possibility of bulge occurrence in actual situations, using an in-house computer code, in which the implicit time-integration scheme, calibrated by the Runge-Kutta [21], [22] high-order method, is employed with the aid of the Newton-Raphson linearization method [23], [24].

## II. FORMULATION

After the time-and-space discretization of terms representing temporal concentrations, drift, but prior to the linearization, two carrier transport equations [25]–[28] and Poisson equation [7], [29] are derived as

$$\gamma_{ni}\left(n - n_i^p\right) = \left[\left(V_{i-1} - V_i\right)\left(n_{i-1} + n_i\right) - \left(V_i - V_{i+1}\right) \times \left(n_i + n_{i+1}\right)\right] + \beta_n\left(n_{i-1} - 2n_i + n_{i+1}\right), \quad (1)$$

$$\gamma_{pi}\left(p - p_i^p\right) = \left[-\left(V_{i-1} - V_i\right)\left(p_{i-1} + p_i\right) + \left(V_i - V_{i+1}\right) \times \left(p_i + p_{i+1}\right)\right] + \beta_p\left(p_{i-1} - 2p_i + p_{i+1}\right), \quad (2)$$

And

$$V_{i-1} - 2V_i + V_{i+1} + \gamma_V\left(p_i - n_i + N_D - N_A\right) = 0 \quad (3)$$

where $\gamma_n = \left(2\left(\Delta x\right)^2\right)/\left(\mu_n \Delta t\right)$, $\beta_n = \left(2D_n\right)/\mu_n$, $\gamma_p = \left(2\left(\Delta x\right)^2\right)/\left(\mu_p \Delta t\right)$, $\beta_p = \left(2D_p\right)/\mu_p$, and $\gamma_V = \left(q\left(\Delta x\right)^2\right)/\varepsilon_s$. Subsequently, $n$ denotes electron concentration; $D_n$ electron diffusion coefficient; $\mu_n$ electron mobility; $p$ hole concentration; $D_p$ hole diffusion coefficient; $\mu_p$ hole mobility; $V$ voltage; $q$ elementary charge; $\varepsilon_s$ semiconductor permittivity; $N_D$ donor-impurity density; $N_A$ accepter-impurity density; and $i$ the index for node i. The superscript $p$ denotes "value at the previous time step". These three nonlinear algebraic equations are subject to the initial condition (at $t = 0$) : $p = N_A, n = n_{i0}^2/N_A$ for $0 < \mathrm{x} < x_{int}$ and $p = n_{i0}^2/N_D, n = N_D$ for $x_{int} < \mathrm{x} < \mathrm{L}$ as well as the boundary condition (for $t > 0$): $p = N_A, n = n_{i0}^2/N_A, dV/dx = 0$ at $x = 0$ and $p = n_{i0}^2/N_D, n = N_D$, $dV/dx = 0$ at $x = L$, where $n_{i0}$ denotes the intrinsic carrier concentration; subscript "int" the interface.

We have adopted the central (as opposed to upwind) finite difference method to discretize drift terms because of our fear of introducing the unnecessary numerical accuracy. Then these equations are linearized and simultaneously solved using the Newton-Raphson method. As p carriers behave similarly, only the transient spatial distributions of n carriers are displayed in 3D graphics (Fig. 1). At $t = t_1$, the bulge appears. At $t = t_{max}$, the swelling height reaches its maximum. At $t = t_2$, the bulge gradually subsides. Finally, at $t = t_{ss}$ (ss: steady state), it completely diminishes, and

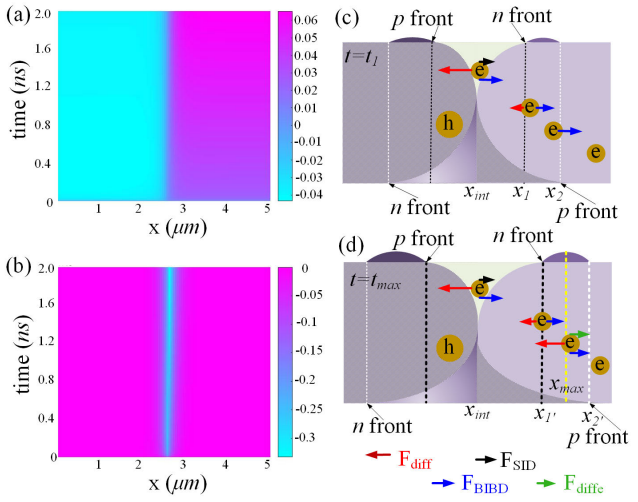


**FIGURE 2. Forces exerted on electrons at different times and locations. a, temporal and spatial voltage (V, in units of volt) with the color bar indicating the its value. b, temporal and spatial electrical field intensity (E, in units of volt per meter) with the color bar indicating the its value. c, The bulge starts to appear at $t = t_1$. In principle, it starts immediately after $t = 0$, but does not appear conspicuous in early times. d, The instant when the swelling height reaches its maximum. The subscript "diffe" stands for "diffusion force eastbound".**

the steady state is attained. More explanations will be given in Fig. 2 below.

## III. PHENOMENON AND THEORY OF CARRIER BULGES

This study has detected transient occurrences of seemingly law-defying bulges in carrier spatial distributions after doping processes. Intuitively, the electron concentration can at most reach $n_0$, but should by no means protrude into a bulge. Our thoughts prompted us to conduct simulations on diffusion-drift problems for single carriers only. As predicted, absolutely no bulges emerge in single-carrier transient distributions (Fig. 1b), thus provoking a possibility that such bulges are mysteriously induced by the involvement of the transport of the other carrier. Our quest seeking for logical explanations ensued. Below it is elaborated in three steps that explain the bulge occurrence.

### A. SINGLE-CARRIER IN N-TYPE SEMICONDUCTOR (STEP 1)

Consider transient transports of electrons inside the n-type semiconductor (Fig. 1b revisited) at five instants in the absence of hole-carrier movements. During $0 < t < t_{ss}$, the diffusion takes place, with its rate at $x_{int}$ decreasing monotonically.

At $t = t_1$, while electrons diffuse westbound, the front, defined as the location where the n carrier concentration lowers from 100% of $N_D$ to 99.99% in the n-type semiconductor ($x = x_f$; "f" stands for "front"), moves eastbound. The drift starts as soon as the diffusion starts, and acts as an opposing aftereffect of the diffusion.

At $t = t_2$ and $x = x_{int}$, the $n$ concentration decreases to 55% of $N_D$, with its rate equaling -4.19 × $10^5$ C/(m$^2$s), which is greater than the drift rate 3.71 × $10^5$ C/(m$^2$s), implying that both processes will continue spontaneously.

At $t = t_3$, the spatial distribution looks qualitatively similar to that at $t = t_2$, and is included redundantly herein merely for the sake of cosmetic alignment with the binary-diffusion case shown above.

At $t = t_{ss}$, diffusion ≈ −4.43×$10^5$ C/(m$^2$s), drift ≈ 4.43× $10^5$ C/(m$^2$s), and both mechanisms balance each other. The conservation of n-carrier concentration is governed by

$$\Delta x \left(n_i - n_i^p\right)/\Delta t = C_e - C_w, \tag{4}$$

where $C_e = \mu_n n_e E_e + D_n \left(\Delta n/\Delta x\right)_e$ and $C_w = \mu_n n_w E_w + D_n \left(\Delta n/\Delta x\right)_w$ represent concentration fluxes at locations $e$ (east) of the control volume and $w$ (west) of the control volume; $p$ the previous time step; $E$ the electrical field; $i$ the number of the control volume. Thus, Eq. (4) becomes

$$n_i - n_i^p \propto \mu_n \left(n_e E_e - n_w E_w\right) + D_n \left(\left(\Delta n/\Delta x\right)_e - \left(\Delta n/\Delta x\right)_w\right), \tag{5}$$

where $\Delta n_e = n(i+1) - n(i)$; $\Delta n_w = n(i) - n(i-1)$. Letting $n_w = n_e - \gamma$, with $\gamma > 0$, authors can further rearrange the nonlinear term in the right-hand side of Eq. (5) into $n_e (E_e - E_w) + \gamma E_w$ or $n_e q(N_D - n_i)/\varepsilon_s$, where $E_e - E_w = \Delta x q(N_D - n_i)/\varepsilon_s$ according to Poisson equation and $\varepsilon_s$ denotes the dielectric constant. Consequently, for clarity, Eq. (5) can be rewritten as

$$n_i - n_i^p \propto source + sinkI + sinkII, \tag{6}$$

where $source = n_e q\left(N_D - n_i\right)/\varepsilon_s > 0$; $sinkI = \gamma E_w < 0$ because $E$ acts westward throughout the entire domain and is negative; $sinkII = \left(\Delta n/\Delta x\right)_e - \left(\Delta n/\Delta x\right)_w < 0$ in the n-type semiconductor, lowering $n(t, x)$ and thus behaving as a sink. Consequently, $n$ cannot possibly exceed $N_D$, and neither can bulges possibly emerge.

### B. DEMONSTRATION OF THE EARLY ARRIVAL OF THE N CARRIER IN P JUNCTION (STEP 2)

The drift term, being proportional to $nE$, is contained in the $n$-carrier transport equation. Since $E$ lies in the similar order of magnitudes in p-type and n-type semiconductors, the strength of the drift is primarily proportional to $n$, which, by contrast, varies several orders of magnitudes across the depletion zone. However, the value of the minority $n$ carrier in p-type segment is much smaller than that of the majority $n$ carrier in n-type semiconductor, authors conclude that smaller source terms exist in p-type semiconductor, leading to weaker opposing forces to the diffusion process, and thus greater front moving speeds. In this example, $n$ carrier spatial distribution is prescribed as $n = n_{i0}^2/N_A$ for $0 \le x \le x_{int}$ and $n = N_D$ for $x_{int} \le x \le L$, respectively (inset of Fig. 3). The spatial distribution of $n$ carrier at $t = t_1$ shows arrivals of the front at $x = x_{n1}$ and the front at $x = x_{n2}$, respectively (Fig. 3).

**TABLE 1.** Comparison of magnitudes of all mechanisms. It is necessary to retain long strings of decimal places because the numerical accuracy will be lost if we truncate tails of those strings. Unit ($cm^{-3}/s$).

| $dn/dt$ | Source by self | Source by binary | SinkI | SinkII |
|---|---|---|---|---|
| $-4.9275\times10^{23}$ | $3.7803\times10^{25}$ | $1.2626\times10^{25}$ | $-1.8115\times10^{25}$ | $-3.2806\times10^{25}$ |

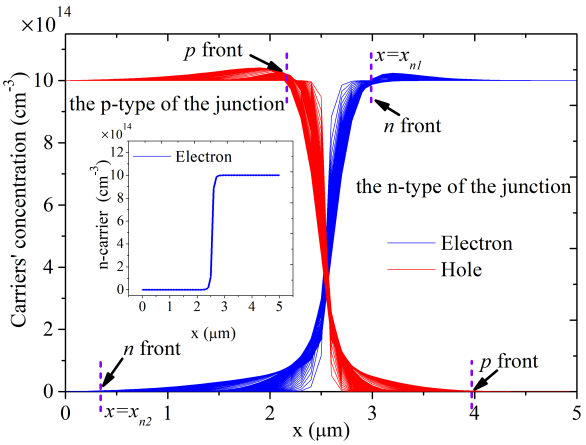


**FIGURE 3.** The contrast of fronts' traveling speeds. The left n front travels faster in the p-type of the junction than the right n front does in the n-type of the junction (at $t$= 125$ps$).

### C. BULGE-INDUCING BINARY DIFFUSION (BIBD) IN P/N JUNCTION (STEP 3)

Finally, this step can be viewed as the crux of the present work. Let us now examine the binary-diffusion phenomenon with the focus on explaining the transport phenomena taking place in the n-type theater (Fig. 2, which corresponds to Fig. 1a with sub-figures at $t = t_1$ and $t = t_{max}$. Those taking place in the p-type theater can be described similarly and are omitted.

At $=$ 0, or at the instant of freshly completing the doping process (actual situations will be discussed in the part: the possibility of bulge occurrence), the voltage and electrical field intensity both equal zero throughout the n-type semiconductor (Figs. 2a and 2b), therefore no forces act on electrons at this instant.

At $t = t_1$ (Fig. 2c), the $n$-carrier front arrives at $x = x_1$ and the $p$-carrier front has already arrived at $x = x_2$ (see the green curve in the n-type theater). Equation (6) remains valid, except that now

$$source = n_e q(N_D - n_i)/\varepsilon_s + n_e q(p - N_A)/\varepsilon_s, \qquad (7)$$

whose first term, explained in logical step 1, exerts no effects on bulges. The second term, behaving as a source ($p > N_A$ in n-type semiconductor), contributes most critically to the bulge-inducing binary diffusion (BIBD) effect. Dynamically, an electron at $x = x_{int}$ is exerted by three forces, namely, the "diffusive force" ($F_{diff}$, which is fictitious), the self-induced-drift force ($F_{SID}$, and the BIBD force ($F_{BIBD}$). Note that $F_{diff}$ is greater than the sum of $F_{SID}$ and $F_{BIBD}$, so that this electron, subject to a net westward resultant force, will continue to move westward. At $x = x_1$, the electron is exerted by two forces only, namely $F_{diff}$ and $F_{BIBD}$. The arrival of the minority $p$-carrier front has taken place, inducing $E$. So does the onset of the diffusive force. The $F_{SID}$ is absent because $n = N_D$, and the first term in Eq. (7) vanishes. At $x = x_2$, the electron is exerted by $F_{BIBD}$ only. For $x > x_1$,, the $n$-carrier front has not arrived. Therefore, neither $F_{diff}$ nor the $F_{SID}$ exist. However, due to the presence of $F_{BIBD}$, a mild bulge appears as shown. It is interesting to determine magnitudes of all mechanisms at a location between $x_1$ and $x_2$ (Table 1).

At $t = t_{max}$ (Fig. 2d), situations for electrons at $x = x_{int}$ are similar to those at $x = x_{int}$ and $t = t_1$. Situations for electrons at $x = x_{1'}$ are similar to those at $x = x_1$ and $t = t_1$. At $x = x_{max}$, three forces act on electrons. Among them, the force $F_{diffe}$ represents the diffusive force due to the bulge, but not due to the regular monotonic spatial distribution. Looking at the right slope of the bulge, authors notice that the concentration spatial gradient, $\partial n/\partial t$, is now negative. Hence this fictitious diffusive force acts eastbound and is positive, unlike regular westbound diffusive forces. It is this force that behaves as a sink and helps to suppress the bulge as the system approaches the steady state.

At $t = t_{ss}$, all electrons in the depletion zone are uniformly subject to three forces, namely, $F_{diff}$, $F_{SID}$, and $F_{BIBD}$, which are balanced to net zero. The bulge has subsided, and finally diminished. In dynamic equilibrium, the number of diffusive electrons (moving westbound) equals the number of drift electrons (moving eastbound) at every $x$ location.

## IV. EXPERIMENTAL RESULTS IN STEADY-STATES

For steady states, we have managed to conduct experiments using the spreading resistance profiling technique to measure both resistivity and resistance distributions of the p/n junction, and subsequently deduce the hole concentration in the p-type theater and the electron concentration in the n-type theater (Fig. 4a). According to the spreading resistance profiling principle, experimenter measures the resistance between two probes and deduces the carrier concentration, then can obtain carrier distribution of different depth through dealing with the bevel surface (bevel angle). The measured p/n junction device is fabricated on silicon substrate doped with P and Mg. This experimental carrier-concentration distribution in steady state (Fig. 4a), when qualitatively compared with the simulation counterpart that is calculated in steady state (steady-state simulation code), offers authors the guidance in choosing proper parametric values of system sizes, p/n material intrinsic concentrations. It is understandably difficult for authors to strive for satisfactory agreements because defects of micro-gaps and micro-holes

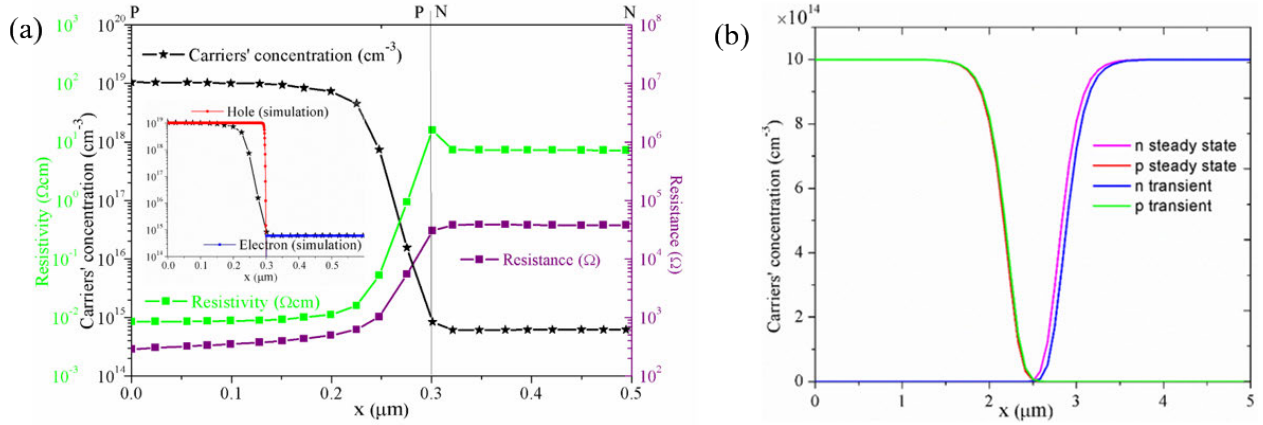


**FIGURE 4.** Results of experiment and simulation. (a) The black line denotes the carriers' concentration (cm-3), green line resistivity (Ω-cm), and purple line resistance (Ω). The black line in p-type semiconductor stands for the hole's concentration; the black line in n-type semiconductor stands for the electron's concentration. Red and blue lines denote hole's and electron's concentrations by simulations, respectively, whereas the black line stands for carriers' concentration by experiments. Since the ordinate is marked in the logarithmic scale as well as all nodal residuals have been carefully checked (Tables 1 and 2), the display of those sharp right-angle corners that exist inside the depletion zone should not alarm us. (b) The steady-state carrier concentration computed by the steady-state simulation code is compared with the transient result computed by the transient code at $t = 100\ \mu$s. The 'n steady state' denotes electron concentration computed by steady state code; 'p steady state' denotes hole concentration computed by steady state code; 'n transient' denotes electron concentration computed by transient code; 'p transient' denotes hole concentration computed by transient code.

**TABLE 2.** Confirmation of the bug-free status in the simulation code. The reason of retaining long strings of decimal places is the same as that stated in Table 1. Unit ($cm^{-3}/s$).

| $dn/dt$ | drift | diffusion | Resm |
|---|---|---|---|
| $-1.7598\times10^{24}$ | $3.9089\times10^{25}$ | $-4.0849\times10^{25}$ | $2.7022\times10^{11}$ |

inevitably exist in lab samples. Therefore, it can be thought that simulation results are consistent with experimental data in the steady state. In Fig. 4b, steady-state carrier concentrations computed by the steady-state simulation code are compared with the transient result computed by the transient code at $t = 100\ \mu$s. As observed, hole concentrations agree almost identically, whereas electron concentrations differ only slightly. These agreements validate our simulation codes and support the occurrences of carrier-concentration transient bulges.

Simulation results of bulge peaks in the transient state are plotted versus the time in nanoseconds (Fig. 5) with the inset showing conspicuous bulged variations parameterized in dopant amount. In addition, it is intriguing to observe that a sharp maximal peak exists and occurs in the region of small dopant amounts (Fig. 5 inset). The reason lies in that, for small dopant amounts, carriers diffuse slowly, prolonging the time that is required for the system to reach the steady state. Since the transient duration is prolonged, the electrical field induced by the minority-carrier front also acquires the chance of lingering in the bulge regime for a long time, causing extremely protruding bulges (as protruding as 4.1%).

At a typical time and location (e. g. $t = 74ps$ and $x = 3.5\mu m$), we obtain $dn/dt = 2.1\times10^{23}cm^{-3}/s$, whereas the recombination rate can be estimated to be $(n_n - N_D)/\tau_n = 3.45\times10^{14}cm^{-3}/s$ in the absence of external voltages ($\tau_n$ recombination carrier lifetime), implying that the effect of the recombination rate can be safely neglected in the present study.

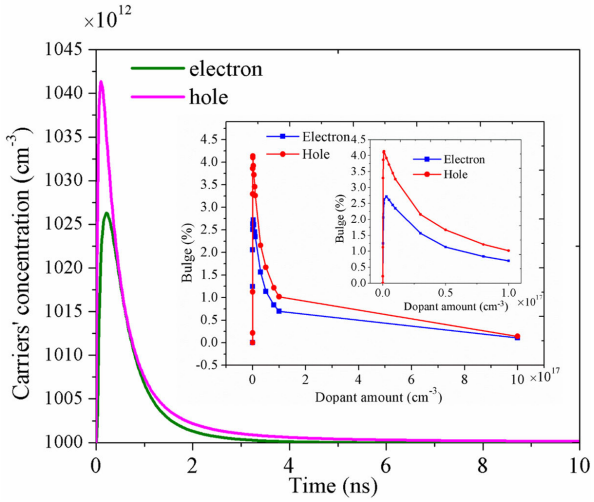


**FIGURE 5.** Simulation results of bulge peaks in the transient state versus the time in nanoseconds ($N_D = 10^{15}cm^{-3}, N_A = 10^{15}cm^{-3}$) and the bulge height as a function of the dopant amount. In the proposed study, $N_D = N_A$ for silicon p/n junctions.

## V. THE POSSIBILITY OF BULGE OCCURRENCE IN ACTUAL SITUATIONS

### A. DURING DOPING PROCESS

In our simulations, the initial condition is somewhat idealized. In actual doping processes, the bulged phenomenon will only happen under the condition that the doping rate exceeds the bulge rate. Here the doping rate is defined as the doping penetration depth per unit time, whereas the

bulge rate denotes the transverse distance traveled by the bulge per unit time. For example, consider the case in which a p-type semiconductor flux is doped into an n-type semiconductor. When the minority-p front moves ahead of the majority-n front in the n-type semiconductor, an electrical field is generated, as shown in Fig. 2c and 2d. It is exactly this electrical field that persists sufficiently long to allow bulges to be generated. Under the condition of $N_D = 10^{15} cm^{-3}$ and $N_A = 10^{15} cm^{-3}$, the bulge rate is 458.72m/s (380.79m/s for the case in which an n-type semiconductor flux is doped into a p-type semiconductor). Since it is difficult to dope semiconductors in high doping velocities without defects, it may be equally difficult for these bulges to be detected in experiments conducted in the current doping technology.

### B. FORWARD BIASED VOLTAGE

When the p/n junction is abruptly driven by forward-biased voltage, oppositely to the direction of the electric field induced by the diffusion front, this forward-biased voltage will counteract this electric field, thus suppressing the occurrence of the bulge.

### C. REVERSE BIASED VOLTAGE

When the junction is abruptly driven by reverse-biased voltage, this voltage will weaken carrier-diffusion fluxes, subsequently weakening the electric field and thus also suppressing the occurrence of the bulge.

## VI. CONCLUSIONS

Occurrences of unusual bulges in transient carrier spatial distributions are discovered, but rigorously validated by computational simulations, aided by experimental data guiding our choices of parametric values. These bulges confine electrons both locally and instantaneously (for several nanoseconds). Step-by-step, this research offers explanations of the governing mechanism, which is abbreviated as BIBD. These transient bulges can be observed if the doping rate surpasses the bulge rate. No bulges occur in cases of forward- and reverse-driven voltages. This discovery of bulges and BIBD mechanism may help understand characteristics of semiconductor devices in transient state.

## REFERENCES

[1] H. J. Queisser, H. C. Casey, and W. van Roosbroeck, "Carrier transport and potential distributions for a semiconductor p-n junction in the relaxation regime," *Phys. Rev. Lett.*, vol. 26, no. 10, p. 551, Mar. 1971, doi: 10.1103/PhysRevLett.26.551.

[2] M. Kantner and T. Koprucki, "Numerical simulation of carrier transport in semiconductor devices at cryogenic temperatures," *Opt. Quantum Electron.*, vol. 48, no. 12, p. 543, Dec. 2016, doi: 10.1007/s11082-016-0817-2.

[3] H. Fardi, "Numerical analysis of semiconductor PN junctions using MATLABTM," *J. Sci. Res. Rep.*, vol. 6, no. 2, pp. 84–98, Jan. 2015, doi: 10.9734/JSRR/2015/14434.

[4] P. González, A. Godoy, F. Gámiz, and J. A. Carrillo, "Accurate deterministic numerical simulation of p-n junctions," *J. Comput. Electron.*, vol. 3, nos. 3–4, pp. 235–238, Oct. 2004, doi: 10.1007/s10825-004-7052-y.

[5] G. Blaj, C. J. Kenney, J. Segal, and G. Haller, "Analytical solutions of transient drift-diffusion in p-n junction pixel sensors," 2017, *arXiv:1706.01429*. [Online]. Available: http://arxiv.org/abs/1706.01429

[6] M. T. Khan, V. Agrawal, A. Almohammedi, and V. Gupta, "Effect of traps on the charge transport in semiconducting polymer PCDTBT," *Solid State Electron.*, vol. 145, pp. 499–53, Jul. 2018, doi: 10.1016/j.sse.2018.04.005.

[7] S. M. Sze, *Semiconductor Devices: Physics and Technology*. New York, NY, USA: Wiley, 2002, Ch. 3.

[8] J. H. Van Der Merwe, "Misfit dislocations in epitaxy," *Metall. Mater. Trans. A*, vol. 33, no. 8, pp. 2475–2483, Aug. 2002, doi: 10.1007/s11661-002-0369-x.

[9] A. Ponchet, G. Patriarche, J. B. Rodriguez, L. Cerutti, and E. Tournié, "Interface energy analysis of III–V islands on Si (001) in the Volmer-Weber growth mode," *Appl. Phys. Lett.*, vol. 113, no. 19, Nov. 2018, Art. no. 191601, doi: 10.1063/1.5055056.

[10] H. J. Scheel, "Historical aspects of crystal growth technology," *J. Cryst. Growth.*, vol. 211, nos. 1–4, pp. 1–12, Apr. 2000, doi: 10.1016/S0022-0248(99)00780-0.

[11] N. M. Gabor, J. C. W. Song, Q. Ma, N. L. Nair, T. Taychatanapat, K. Watanabe, T. Taniguchi, L. S. Levitov, and P. Jarillo-Herrero, "Hot carrier-assisted intrinsic photoresponse in graphene," *Science*, vol. 334, no. 6056, pp. 648–652, Nov. 2011, doi: 10.1126/science.1211384.

[12] K. S. Novoselov, "Electric field effect in atomically thin carbon films," *Science*, vol. 306, no. 5696, pp. 666–669, Oct. 2004, doi: 10.1126/science.1102896.

[13] S. Tongay, K. Berke, M. Lemaitre, Z. Nasrollahi, D. B. Tanner, A. F. Hebard, and B. R. Appleton, "Stable hole doping of graphene for low electrical resistance and high optical transparency," *Nanotechnology*, vol. 22, no. 42, Sep. 2011, Art. no. 425701, doi: 10.1088/0957-4484/22/42/425701.

[14] M. Buscema, D. J. Groenendijk, G. A. Steele, H. S. J. van der Zant, and A. Castellanos-Gomez, "Photovoltaic effect in few-layer black phosphorus PN junctions defined by local electrostatic gating," *Nature Commun.*, vol. 5, no. 1, p. 4651, Dec. 2014, doi: 10.1038/ncomms5651.

[15] X. Yu, S. Zhang, H. Zeng, and Q. J. Wang, "Lateral black phosphorene P–N junctions formed via chemical doping for high performance near-infrared photodetector," *Nano Energy*, vol. 25, pp. 34–41, Jul. 2016, doi: 10.1016/j.nanoen.2016.04.030.

[16] J. Zhang, W. Xie, M. L. Agiorgousis, D.-H. Choe, V. Meunier, X. Xu, J. Zhao, and S. Zhang, "Quantum oscillation in carrier transport in two-dimensional junctions," *Nanoscale*, vol. 10, no. 17, pp. 7912–7917, 2018, doi: 10.1039/C8NR01359D.

[17] F. Zhang, J. Jung, G. A. Fiete, Q. Niu, and A. H. MacDonald, "Spontaneous quantum Hall states in chirally stacked few-layer graphene systems," *Phys. Rev. Lett.*, vol. 106, no. 15, Apr. 2011, Art. no. 156801, doi: 10.1103/PhysRevLett.106.156801.

[18] L. Huang, G. V. Hartland, L.-Q. Chu, Luxmi, R. M. Feenstra, C. Lian, K. Tahy, and H. Xing, "Ultrafast transient absorption microscopy studies of carrier dynamics in epitaxial graphene," *Nano Lett.*, vol. 10, no. 4, pp. 1308–1313, Apr. 2010, doi: 10.1021/nl904106t.

[19] N. Tessler and G. Eisenstein, "Transient carrier dynamics and photon-assisted transport in multiple-quantum-well lasers," *IEEE Photon. Technol. Lett.*, vol. 5, no. 3, pp. 291–293, Mar. 1993, doi: 10.1109/68.205615.

[20] T. Dekorsy, T. Pfeifer, W. Kütt, and H. Kurz, "Subpicosecond carrier transport in GaAs surface-space-charge fields," *Phys. Rev. B, Condens. Matter*, vol. 47, p. 3842, Feb. 1993, doi: 10.1103/PhysRevB.47.3842.

[21] R. L. Honeycutt, "Stochastic Runge-Kutta algorithms. I. White noise," *Phys. Rev. A, Gen. Phys.*, vol. 45, no. 2, p. 600, Jan. 1992, doi: 10.1103/PhysRevA.45.600.

[22] E. Runge and E. Gross, "Density-functional theory for time-dependent systems," *Phys. Rev. Lett.*, vol. 52, no. 12, p. 997, Mar. 1984, doi: 10.1103/PhysRevLett.52.997.

[23] A. Ben-Israel, "A Newton-Raphson method for the solution of systems of equations," *J. Math. Anal. Appl.*, vol. 15, no. 2, pp. 243–252, Aug. 1966, doi: 10.1016/0022-247X(66)90115-6.

[24] T. J. Ypma, "Historical development of the Newton–Raphson method," *SIAM Rev.*, vol. 37, no. 4, pp. 531–551, Dec. 1995, doi: 10.1137/1037125.

[25] P. J. Barneo, J. E. Amaro, and A. M. Lallena, "Nuclear currents based on the integral form of the continuity equation," *Phys. Rev. C*, vol. 60, no. 4, Sep. 1999, Art. no. 044615, doi: 10.1103/PhysRevC.60.044615.

[26] G. Tatara and P. Entel, "Calculation of current-induced torque from spin continuity equation," *Phys. Rev. B, Condens. Matter*, vol. 78, no. 6, Aug. 2008, Art. no. 064429, doi: 10.1103/PhysRevB.78.064429.

[27] H. J. Hovel, *Semiconductors and Semimetals*, vol. 11. New York, NY, USA: Academic, 1975.
[28] C. Jacoboni, C. Canali, G. Otiaviani, and A. A. Quaranta, "A review of some charge transport properties of silicon," *Solid-State Electron.*, vol. 20, pp. 77–89, Feb. 1977, doi: 10.1016/0038-1101(77)90054-5.
[29] A. Gonis, E. C. Sowa, and P. A. Sterne, "Exact treatment of Poisson's equation in solids with space-filling cells," *Phys. Rev. Lett.*, vol. 66, no. 17, p. 2207, Apr. 1991, doi: 10.1103/PhysRevLett.66.2207.

**JIHONG ZHANG** received the B.S. degree in electron science and technology from the China University of Mining and Technology, Xuzhou, China, in 2010, and the Ph.D. degree from the Department of Electronic Science, Xiamen University, China, in 2015. Since 2015, she has been with the School of Electromechanical and Automotive Engineering, Yantai University, where she is currently an Assistant Professor. Her current research interests include onsolid-state lighting, solar cells, and micro nanoscale heat transfer.

**TIENMO SHIH** received the B.S. degree in mechanical engineering from Taiwan University, in 1970, and the Ph.D. degree from the Department of Mechanical Engineering, University of California at Berkeley, in 1977. Afterwards, he became a Postdoctoral Fellow with Harvard University, in 1978. From 1978 to 2012, he taught and conducted research as an Associate Professor with the University of Maryland, College Park. From 2012 to 2018, he was a Professor with the Physics Department, Xiamen University. His current research interests include heat transfer in nanoscales and thermodynamics.